SLAC-PUB-2239
December 1978
(I)

CRITICAL STATE MODEL FOR THE DETERMINATION OF CRITICAL CURRENTS IN DISK-SHAPED SUPERCONDUCTORS *

David J. Frankel
Stanford Linear Accelerator Center, Stanford, CA 94305

ABSTRACT

A series of experiments has been carried out on the flux trapping and shielding capabilities of a flat strip of Nb-Ti/Cu composite material. A circular piece of material from the strip was tested in a uniform field directed perpendicularly to the surface of the sample. Profiles of the normal component of the field along the sample diameter were measured. The critical state model was adapted for this geometry and proved capable of reproducing the measured field profiles. Model curves agreed well with experimental field profiles generated when the full sample was in the critical state, when only a portion of the sample was in the critical state, and when profiles were obtained after the direction of the rate of change of the magnetic field was reversed. The adaptation of the critical state model to the disk geometry provides a possible method either to derive values of the critical current from measurements of field profiles above thin flat samples, or to predict the trapping and shielding behavior of such samples if the critical current is already known. This method of determining critical currents does not require that samples be formed into narrow strips or wires, as is required for direct measurements of J_c, or into tubes or cylinders, as is usually required for magnetization-type measurements. Only a relatively small, approximately circular piece of material is needed. The method relies on induced currents, so there is no need to pass large currents into the sample. The field profile measurements are easily performed with inexpensive Hall probes and do not require detection of the resistive transition of the superconductor.

* Work supported by the Department of Energy, contract No. EY-76-C-03-0515.

I. INTRODUCTION

Bean[1] first introduced the concept of the critical state, in which a superconductor responds to any change in applied field with shielding or trapping currents that flow at the level of the critical current, J_c. These currents flow in the material to whatever depths are required to shield out the field change, and at amplitudes which generally depend on the value of the local field. The concept of the critical state has proved extremely useful in understanding the magnetic behavior of a wide variety of samples. It allows a connection to be made between the microscopic pinning forces of a material, its critical current, J_c, and its macroscopic magnetic behavior.[2,3] In particular, the postulates of the critical state, together with Maxwell's equations and information on $J_c(B)$, have been used to derive expressions for the field distribution and the magnetization of slab-shaped or cylindrical samples in parallel fields.[1,4,5,6] In a few cases, critical state models have been applied to other geometries.[7,8,9] However, in these cases $J_c(B)$ has usually been approximated by J_c = constant, or the configurations have been limited to semi-infinite strips or tubes. In a case involving a flat strip formed into a large loop,[10,11] difficulties were encountered in accounting for results with a critical state model. The present work suggests that the concept of the critical state can be successfully extended to the disk geometry. This extension allows the magnetic behavior of disk-shaped samples to be modeled, and the critical currents of such samples to be determined.

II. CRITICAL STATE MODEL

The magnetic behavior of a disk-shaped sample is somewhat more difficult to analyze than the usual case of a long cylinder in an axial field, where the high degree of symmetry ensures a particularly simple form of the critical

state. In the case of a flat disk in an axial field, the critical currents all flow in the azimuthal direction since the relation $\mu_0 \vec{J} = \nabla \times \vec{B}$ reduces to

$$\mu_0 J_\phi = \left(\frac{\partial B_r}{\partial z} - \frac{\partial B_z}{\partial r} \right) \tag{1}$$

For samples with a large diameter-to-thickness ratio it was possible to use an iterative procedure to obtain self-consistent solutions for the magnetic field and current distribution of a model disk consisting of an array of N coaxial current loops lying in the $z = 0$ plane. Each current loop of the model disk had an effective width, Δr, of 22.86/N mm, and thickness, Δz, of 0.10 mm, equal to the thickness of the superconductor in the sample disk. N was typically greater than 180, resulting in Δr values of less than 0.13 mm. The current $I(r_i)$ flowing in the i^{th} loop was determined by

$$I(r_i) = J_\phi(r_i) \Delta r \Delta z,$$

where $J_\phi(r_i)$ is the current density at the radius r_i of the i^{th} loop. A closed form expression for the z-component of the field at an arbitrary point above a current loop is[12]

$$B_z = \frac{2 \times 10^{-5} I}{\left[(r_i + r)^2 + z^2 \right]^{\frac{1}{2}}} \left[K + \frac{r_i^2 - r^2 - z^2}{(r_i - r)^2 + z^2} E \right] \tag{2}$$

where r_i = radius of the current loop,

(r, z) = location of the observation point,

I = current in the loop,

K, E = complete elliptic integrals of the first and second kind with argument k,

$$k = \frac{4 r_i r}{(r_i + r)^2 + z^2} .$$

This expression was used to calculate the contribution of the series of nested current loops to the field at a distance of 0.76 mm above the plane of the current loops, this being the approximate location of the active area of the Hall probe used to measure the experimental field profiles.

In the first iteration of the model calculation, the field profiles produced by a uniform current distribution, $J_\phi(r_i)$ = constant, or by other simple, arbitrarily specified forms of $J_\phi(r_i)$ were calculated using Eq. 2. The shape of the field profiles generated by a uniform current distribution was in good agreement with the shape of experimental profiles measured at higher fields. In such cases estimates of the critical current level can easily be obtained from the shape of the field profiles or from the maximum field difference maintained across the disk. However, at lower fields where J_c, $\frac{\partial J_c}{\partial B}$, and the total field difference across the disk face are larger, the correspondence between the profiles calculated by assuming J_c = constant and the experimental profiles was not as close. In such cases agreement between model and experimental curves was improved by carrying out further iterations in order to include the effect of the dependence of J_c on B.

In the full form of the model (Figs. 1 and 2), the current distribution in the disk was adjusted iteratively until the current density in every portion of the disk satisfied the criterion of the critical state

$$J_\phi(r_i) = \pm J_c[B_z(r_i)]$$

where $B_z(r_i)$ = z-component of the field at $r = r_i$,

$J_c(B)$ = an assumed form for the relation between the critical current and the local magnetic field.

It was possible to use either an analytic form for $J_c(B)$ or a form of $J_c(B)$

specified by a small table of J_c, B values. For convenience, $J_c = \alpha/B + B_0$ (Kim[5]) was generally employed in the calculations described here. The calculation proceeded using Eq. 2 to obtain the contributions to $\Delta B_z(r_i)$, the field produced by the currents $J_\phi(r_i)$ flowing in the model disk. The effect of an applied field was included by adding a uniform bias field, B_a, to the field generated by the circulating currents. Either trapping or shielding currents were simulated by choosing the appropriate direction of the bias field in relation to the direction of J_ϕ. In the iterative procedure (Fig. 2), the set of field values, $B_z(r_i) = \Delta B_z(r_i) + B_a$, from the n^{th} iteration was used to determine the J_ϕ - values for the $n+1^{th}$ iteration

$$J_\phi(r_i) = J_c(\Delta B_z(r_i) + B_a) . \qquad (3)$$

Starting with an initial estimate of $J_\phi(r_i)$ = constant, the final self-consistent solution, in which Eq. 3 was satisfied for all r_i, was usually obtained within 10 iterations. Changes in the $J_c(B)$ relation caused clearly related changes in the shape of the model field profiles, and the manner in which the trapping or shielding ability of the model disk varied with applied field. For instance, when modeling the flux trapping process, a decrease in α and B_0 resulted in profiles with steeper gradients above the low field outer portions of the disk and flatter gradients above higher field regions near the center of the disk. Smaller B_0 values also resulted in a more rapid decrease in the trapping and shielding ability of the disk with increasing field level.

The generated profiles were insensitive to changes in N, for $N > 100$, as long as z was large compared to the spacing of the loops. The profiles were sensitive to changes in z only near the center and outer edge of the disk; in these areas the magnitude of B_z increased somewhat with decreasing z. In the procedure, the field in the superconducting material is approximated by the

field 0.76 mm above the disk, the location of the scanning Hall probe. In cases where trapping currents are flowing, the effect of this approximation is to underestimate slightly the field used to determine J_ϕ near the center, and to overestimate it slightly near the edge. The reverse effect occurs when shielding currents are flowing. The overall effect of such approximations on the generated field profiles is not expected to be large, since corrections to field values are appreciable only over a limited portion of the disk. Complete verification of the method now requires either more detailed field measurements and analysis to demonstrate the uniqueness of the current distributions, or a careful comparison of disk model results with J_c values derived with conventional critical current measurement techniques.

III. EXPERIMENT

Measurements were carried out in a 63 mm i.d. glass dewar with the sample immersed in liquid helium at 4.2K. The dewar was inserted into a large, water-cooled, 2 T transverse dipole magnet with 0.46 × 0.91 m pole faces, and a 0.10 m gap. As shown in Fig. 3, the disk-shaped sample (A) was clamped in a sample holder (B), supported within the dewar by a long, 12.7mm diameter, thin-walled stainless steel tube (C). The sample was oriented so that the applied field was normal to the plane of the disk. The magnetic field was measured by a 3.2mm square × 0.5mm thick Bell FH-301-040 Hall effect probe (D), with a 1.0mm × 2.0mm active area.[13] The probe was recessed into a thin epoxy-fiberglass strip (E), one end of which was attached to a 6.4mm diameter stainless steel tube (F) concentric with the larger sample support tube. The tube (F) passed through a simple sliding O-ring seal (G) at the top of the support tube. The probe was driven across the face of the sample by a driving mechanism consisting of a 60 rpm reversible motor (H)

connected through a slip clutch (J) to a 104:16 reduction gear (K) and rack and pinion drive (L). The probe position was monitored by a 10-turn potentiometer (M) coupled to the driving mechanism. The probe was calibrated by measuring the field produced by the magnet with a Bell #660 gaussmeter, [13] and then recording the output of the probe as a function of magnet current, either at temperatures above T_c or with the probe moved away from the sample. The probe produced a signal of approximately 140 mV/T at the field levels of interest.

The 45.7 mm diameter, 0.25 mm thick sample consisted of a sandwich of three layers of copper interleaved with two layers of Nb-70at% Ti. [14] The sandwich had been roll-reduced until the layers were approximately 0.05 mm thick and metallurgically bonded to each other. This particular sample was given a 24-hr treatment at 355°C to improve pinning and critical current levels.

Flux trapping experiments were carried out by establishing a magnetic field in the sample while its temperature was above T_c, cooling the sample to 4.2K (or below) while the applied field remained constant, and finally reducing the applied field to zero. Shielding experiments were carried out by cooling the sample in zero field before gradually applying a field. Further data were obtained by cycling the field to its full value and back to zero after a trapping or shielding test was completed. During the experiments, the steady increase or decrease of the applied field was periodically halted and a field profile obtained by moving the Hall probe across the face of the sample. This procedure generated a series of curves of the normal component of the field just above the sample as a function of radial position, at a series of values of the applied field (solid curves in Figs. 4, 5, 6a, and 7).

IV. RESULTS

A series of measured and calculated profiles for cases in which the Nb-Ti disk was in the full critical state is shown in Figs. 4 and 5. In these cases, the procedure of Fig. 2 was used to obtain the fits by modifying the parameters in the $J_c(B)$ expression until good agreement between the model-generated curves and the experimental field profiles was obtained at several field levels. The model field profiles calculated at the lower values of the applied field (particularly the profiles obtained for $B_a = 0$) were quite sensitive to variations in α and B_0 and good fits to the experimental data could be obtained only for $\alpha \cong 1.2 \pm 0.2 \times 10^9$, $B_0 \cong 0.27 \pm 0.1$. At higher fields variations in the shape of individual profiles with changes in α, B_0 were less prominent, although it was possible to constrain the values of α and B_0 further by requiring agreement between model and experimental profiles obtained over a range of field of several times B_0. As shown in the figures, field profiles observed in both increasing and decreasing fields have been reproduced quite well by the model with one set of values for the two adjustable parameters. The disagreement near $r = 0$ was probably due to a small off-center shift in the path of the Hall probe.

Modeling of the curves taken before the field changes had penetrated to the center of the disk (Fig. 6a) required further assumptions about the critical current pattern. It was evident that the entire sample did not enter the critical state until the flux front penetrated to the center of the disk. However, the sample's behavior could not be reproduced by allowing currents to flow only in regions where large scale flux penetration was apparent. Field profiles were calculated for a wide variety of trial current distributions, but good agreement with the experimental curves was obtained only with a current distribution in

which J_ϕ was nonzero at small values of r. The fits to the data shown in Fig. 6a were obtained by interactively modifying the current distribution after each iteration according to the correspondence between the experimental and model curves. This procedure led to current distributions in which $I(r_i)$ was a monotonically decreasing nonzero function of r across the inner portion of the disk. The results of these model calculations were brought into correspondence with the postulates of the critical state by assuming that the shielding currents flowed at $J = J_c(B)$ in a thickness of material that decreased with decreasing radius

$$z = \frac{I(r_i)}{\Delta r \; J_c(\Delta B_z(r_i) + B_a)} \quad .$$

Because of this additional variable it was possible in the partially penetrated case for J(r) and $J_c(B)$ to be varied independently and still obtain fits to the data. However, in practice $J_c(B)$ was first determined by fitting the model curves to data for the fully penetrated case, and then z(r) was determined from the $I(r_i)$ distribution obtained as described above. Figure 6b shows plots of the depth of penetration of the critical state currents as a function of radius obtained with this procedure.

A third type of situation arose when profiles were recorded after the direction of dB_a/dt had been changed. An example of this situation is shown in Fig. 7, where the experimental curves were obtained by applying an increasing field to the sample after a field had been trapped. In such cases, the experimental curves were reproduced by assuming that the change in dB_a/dt caused the critical currents near the outer surface of the disk to reverse direction, while currents flowing in the interior of the material remained unchanged. Good agreement between experimental profiles and model-generated profiles

was obtained when all the currents in the region where dB_z/dr had changed sign reversed direction, and a decreasing proportion of the current flowing at smaller radii was reversed. For example, good correspondence was obtained between the model-generated curve (dashed curve in Fig. 7) and the experimental curve by assuming that all currents at $r > 7.9$ mm and currents flowing in the region $|z| > 0.06$ mm, $r < 7.9$ mm reversed direction, while currents in the remaining portion of the interior of the sample flowed in the original (trapping) direction. In this configuration all currents still obeyed the criteria of the critical state (Eq. 3). As B_a continued to increase, the current distribution changed in a continuous manner from one in which the disk was filled with trapping currents $+J_c$, to a configuration with shielding currents $-J_c$.

V. DISCUSSION

For cases in which the sample is exposed to a monotonic increase or decrease in the applied field, and is fully in the critical state, a relatively simple critical current distribution can account for the experimental results. In such cases, azimuthal currents at a value determined by the local value of B flow throughout the sample, and a straightforward procedure can be used to find the values of these currents from the measured field profiles. The only adjustable parameters required in this procedure are the constants in the $J_c(B)$ expression.

In cases where only a portion of the sample is in the critical state, the distribution of the critical currents is more complicated, and the extent of the sample carrying critical currents as well as the parameters in the $J_c(B)$ expression must be varied in order to reproduce the experimental data. The model calculations indicate that currents must flow in an extended region in the disk above which the axial field is less than 5% of the applied field. These

currents cannot be attributed to the reversible magnetization of the material, since similar behavior was observed when an applied field was decreased after the disk was cooled in a 340 mT field. In such cases, the reversible magnetization acts in opposition to the flux trapping process. Equation 1 can therefore be satisfied only if there is a change in B_r in the material of the order of a few tens of millitesla. Apparently, before the disk enters the full critical state an appreciable radial field is present in those central portions of the disk in which the critical currents are flowing. The critical state is also complex after the direction of the field change has been recently reversed. However, the experimental curves can be reasonably well reproduced by assuming that the change in dB_a/dt causes a total reversal of the currents at the outer radii of the sample, and a partial reversal at smaller radii.

It should be noted that since the radial component of the field was not measured it is not possible to show that the current distributions deduced here are the only possible solutions. The results obtained so far show that current distributions consistent with the postulates of the critical state can provide good correspondence with experimental data on the normal component of the field above a disk sample in the full critical state. By assuming that the current distributions change with changes in the applied fields in a manner similar to the evolution of current distributions in the well-known case of cylindrical samples in axial fields, good correspondence is also obtained with the sample in the partial critical state and after the sample is subjected to changes in the sign of dB_a/dt.

The correspondence between the model and experimental profiles indicates that the analysis of measured field profiles by means of the critical state model provides a prospective method for accurate measurement of critical currents

in disk-shaped superconductors. The method described here offers several potential advantages over customary techniques. It can be used with thin flat samples of almost any size, and, since the method relies on induced currents, it does not require the passage of large transport currents into small samples, or the measurement of small voltages across them. As a result, it is also unnecessary to make a distinction between induced and transport currents. The technique should be particularly useful for determining the critical current level of material used to fabricate flux trapping and shielding devices,[15,16] since these materials are not usually in shapes suited to customary methods of critical current determination. One possible limiting feature of the technique is the occurrence of flux jumps in the material before the full critical state is established. However, in most cases it should be possible to stabilize the material by surrounding it with additional copper, improving cooling conditions, or performing measurements at higher temperatures or fields where stability is improved.

ACKNOWLEDGEMENTS

The author would like to thank Edward L. Garwin and Steve St. Lorant for their helpful discussions of the work. The work was supported by the Department of Energy under Contract No. EY-76-C-03-0515.

REFERENCES

1. C. P. Bean, Phys. Rev. Lett. 8, No. 6, 250 (1962).
2. J. Friedel, P. G. de Gennes, J. Matricon, Appl. Phys. Lett. 2, No. 6, 119 (1963).
3. J. E. Evetts, A. M. Campbell, D. Dew-Hughes, J. Phys. C, Ser. 2, 1, 715 (1968).
4. C. P. Bean, Rev. Mod. Phys. 36, No. 1, 31 (1964).
5. Y. B. Kim, C. F. Hempstead, A. R. Strnad, Phys. Rev. 129, No. 2, 528 (1963).
6. W. A. Fietz, M. R. Beasley, J. Silcox, W. W. Webb, Phys. Rev. 136, No. 2A, A335 (1964).
7. R. Benaroya, H. P. Mogensen, J. Appl. Phys. 37, No. 5, 2162 (1966).
8. S. Shimamoto, Cryogenics 14, No. 12, 641 (1974).
9. W. Witzeling, Cryogenics 16, No. 1, 29 (1976).
10. A. Migliori, R. J. Bartlett, R. D. Taylor, J. Appl. Phys. 47, No. 7, 3266 (1976).
11. A. Migliori, R. D. Traylor, R. J. Bartlett, IEEE Trans. Magn. MAG-13, No. 1, 198 (1977).
12. W. R. Smythe, Static and Dynamic Electricity (McGraw-Hill, New York, 1939), p. 266.
13. F. W. Bell, Inc., Columbus, Ohio.
14. Obtained from Teledyne-Wah Chang Albany, Albany, Oregon.
15. D. J. Frankel, E. L. Garwin, IEEE Trans. Magn. MAG-13, No. 1, 205 (1977).
16. D. J. Frankel, Ph. D. Dissertation, Stanford University (1978). (Also available as Stanford Linear Accelerator Center Report SLAC-211.)

FIGURE CAPTIONS

1. Critical current model for a thin disk in an axial field.
2. Iterative procedure used to determine the critical current from the field profile measurements.
3. Experimental apparatus used to measure the field profiles of the disk-shaped sample.
4. Field profiles obtained in decreasing applied fields (solid curves), and the corresponding model-generated curves (dashed) obtained with $J_c(B) = 1.2 \times 10^9/(B + 0.27)$.
5. Field profiles obtained in increasing applied fields (solid curves), and the corresponding model-generated curves (dashed) obtained with $J_c(B) = 1.2 \times 10^9/(B + 0.27)$.
6. (a) Field profiles obtained in increasing applied fields after the disk was cooled in zero field (solid curves), and the corresponding model-generated curves obtained using the interactive procedure with $J_c(B) = 1.2 \times 10^9/(B + 0.27)$.

   (b) Form for the distribution of the critical currents in the sample that produced the fits shown in (a).
7. Sequence of field profiles generated by applying an increasing field to the sample after a field had been trapped by cooling the sample in a large field and reducing the field to zero.

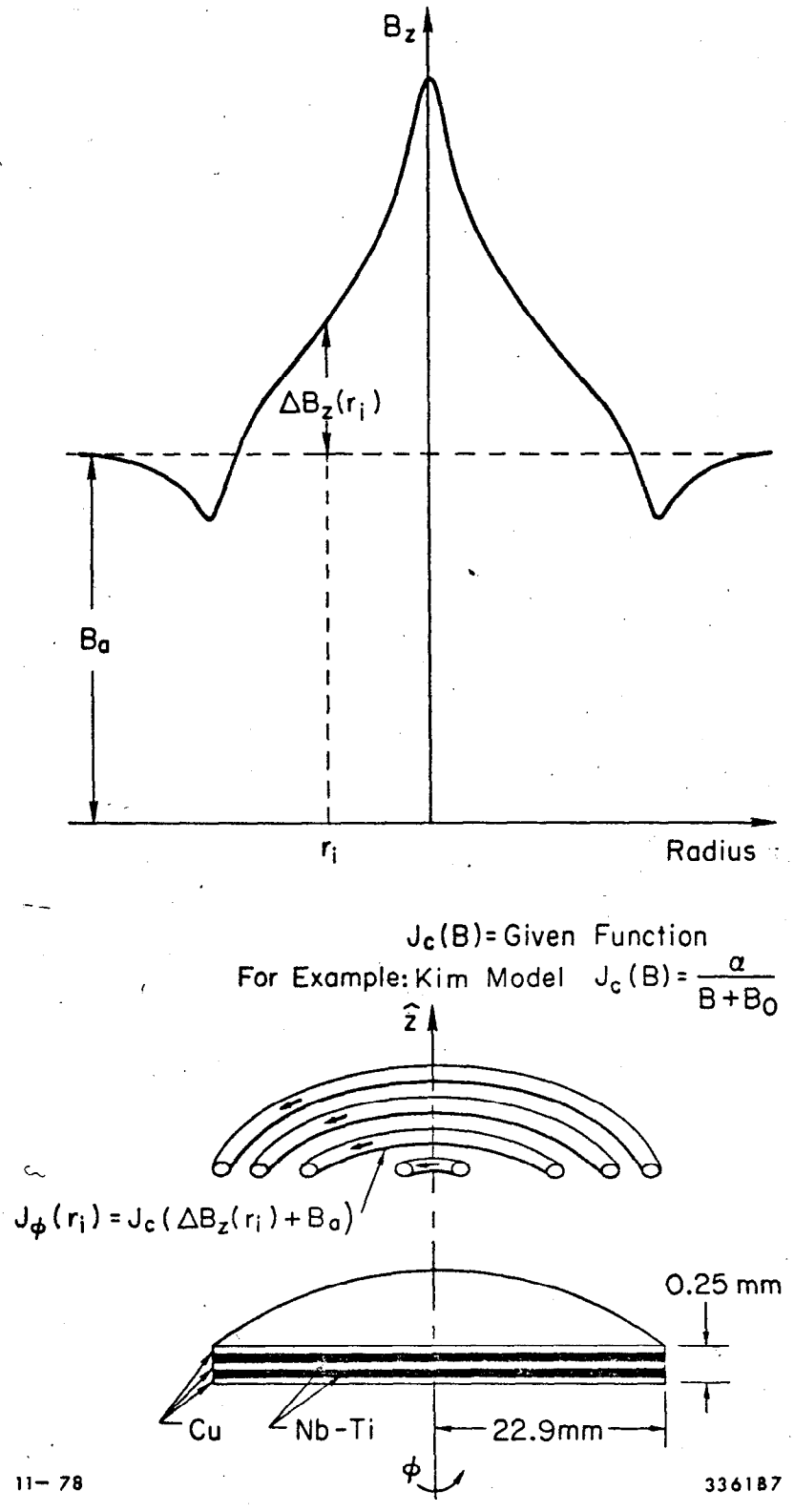
B_z
$\Delta B_z(r_i)$
B_a
r_i
Radius
$J_c(B)$ = Given Function
For Example: Kim Model $J_c(B) = \frac{\alpha}{B+B_0}$
$\hat{z}$
$J_\phi(r_i) = J_c(\Delta B_z(r_i) + B_a)$
0.25 mm
Cu
Nb-Ti
22.9mm
ϕ
11-78
336187

Fig. 1

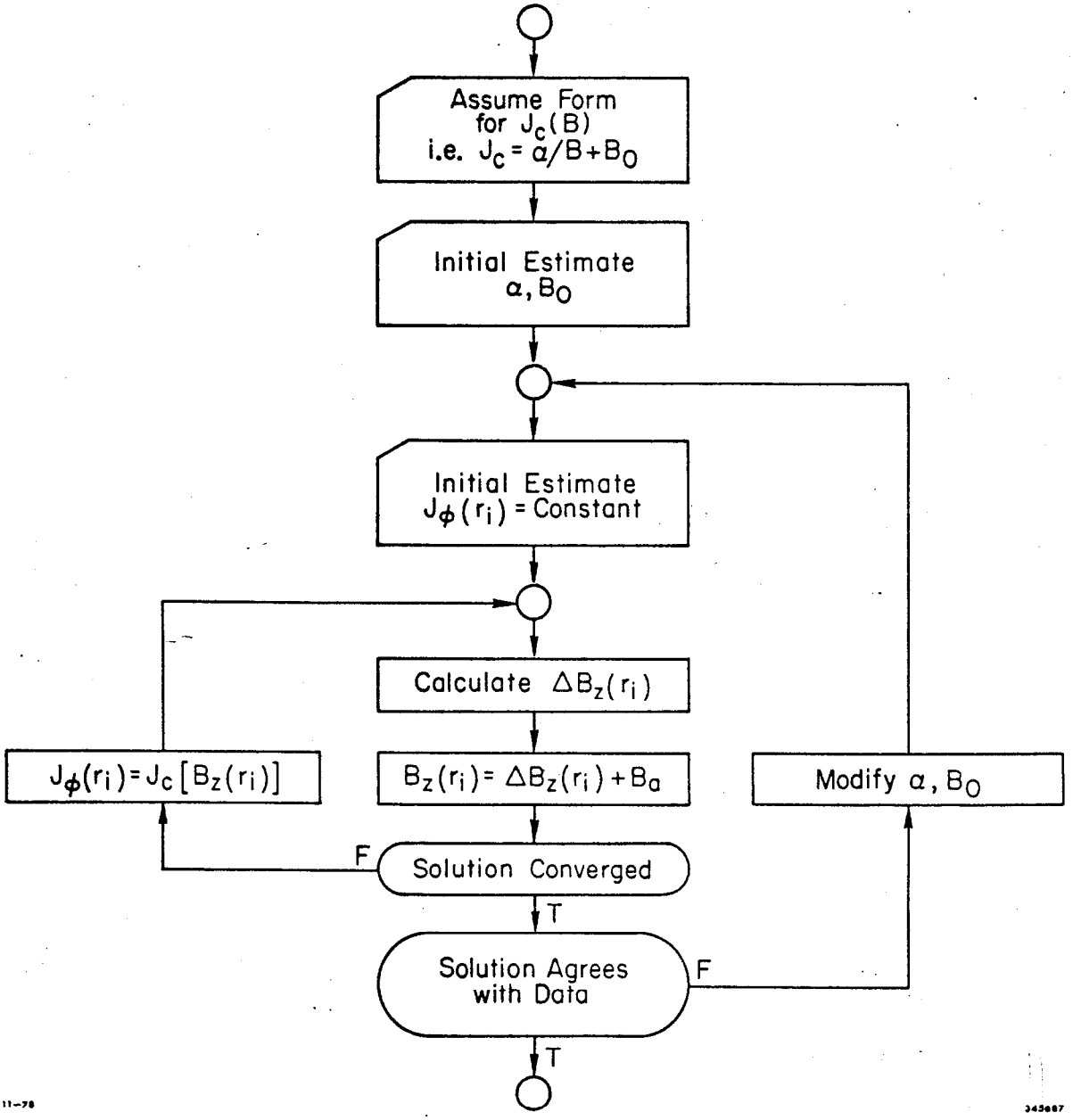
Assume Form for $J_c(B)$ i.e. $J_c = \alpha/B + B_0$
Initial Estimate α, B_0
Initial Estimate $J_\phi(r_i)$ = Constant
Calculate $\Delta B_z(r_i)$
$B_z(r_i) = \Delta B_z(r_i) + B_a$
$J_\phi(r_i) = J_c[B_z(r_i)]$
Modify α, B_0
F
Solution Converged
T
Solution Agrees with Data
F
T

Fig. 2

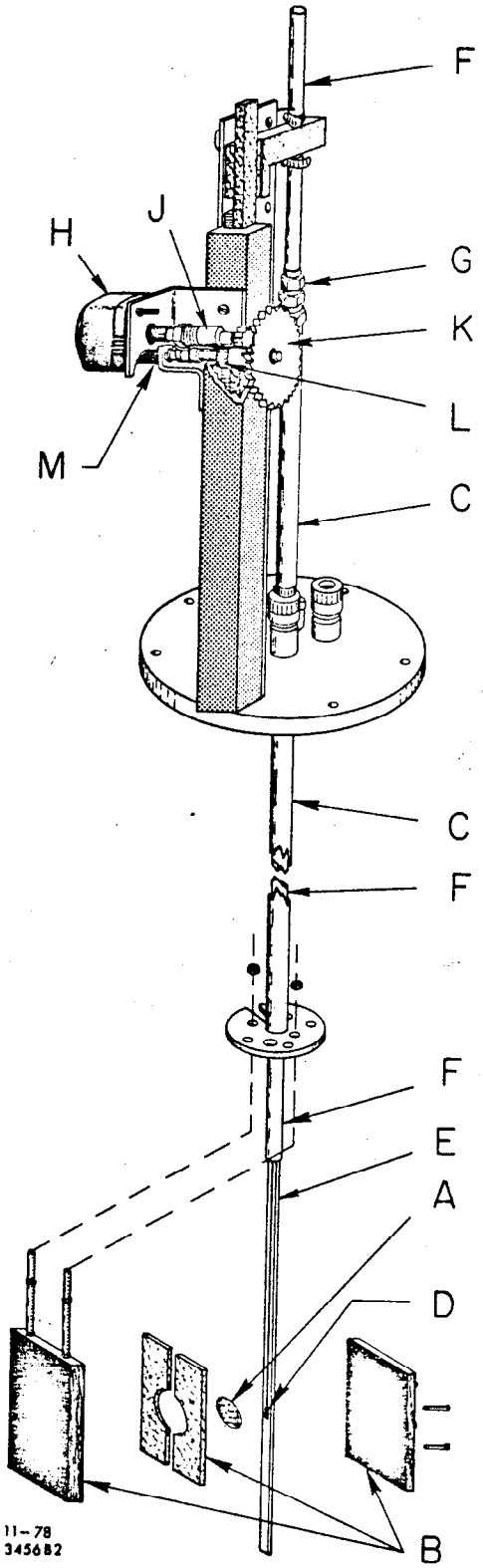

Fig. 3

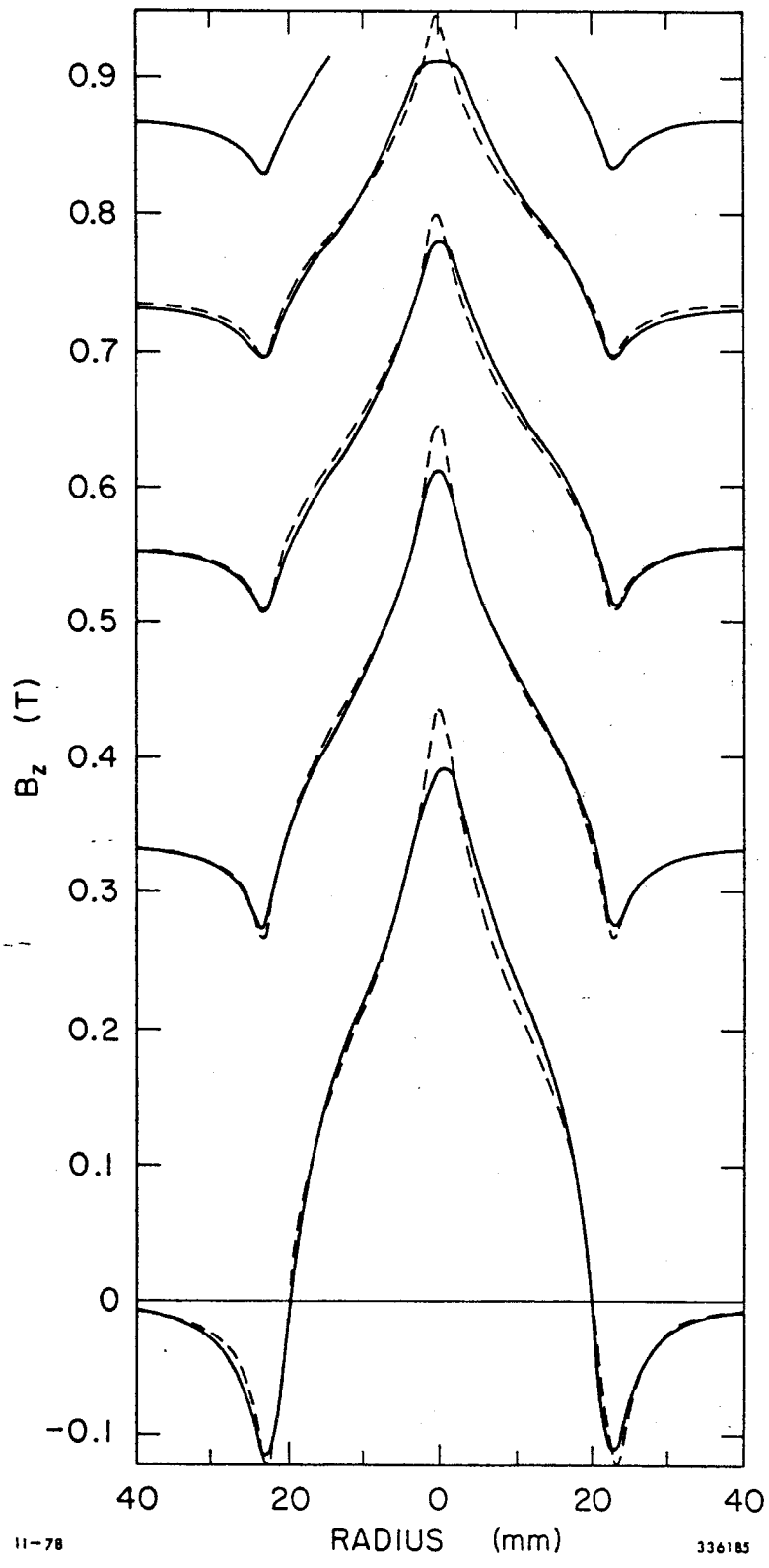
0.9
0.8
0.7
0.6
0.5
0.4
0.3
0.2
0.1
0
-0.1
B_z (T)
40
20
0
20
40
RADIUS (mm)
11-78
336185

Fig. 4

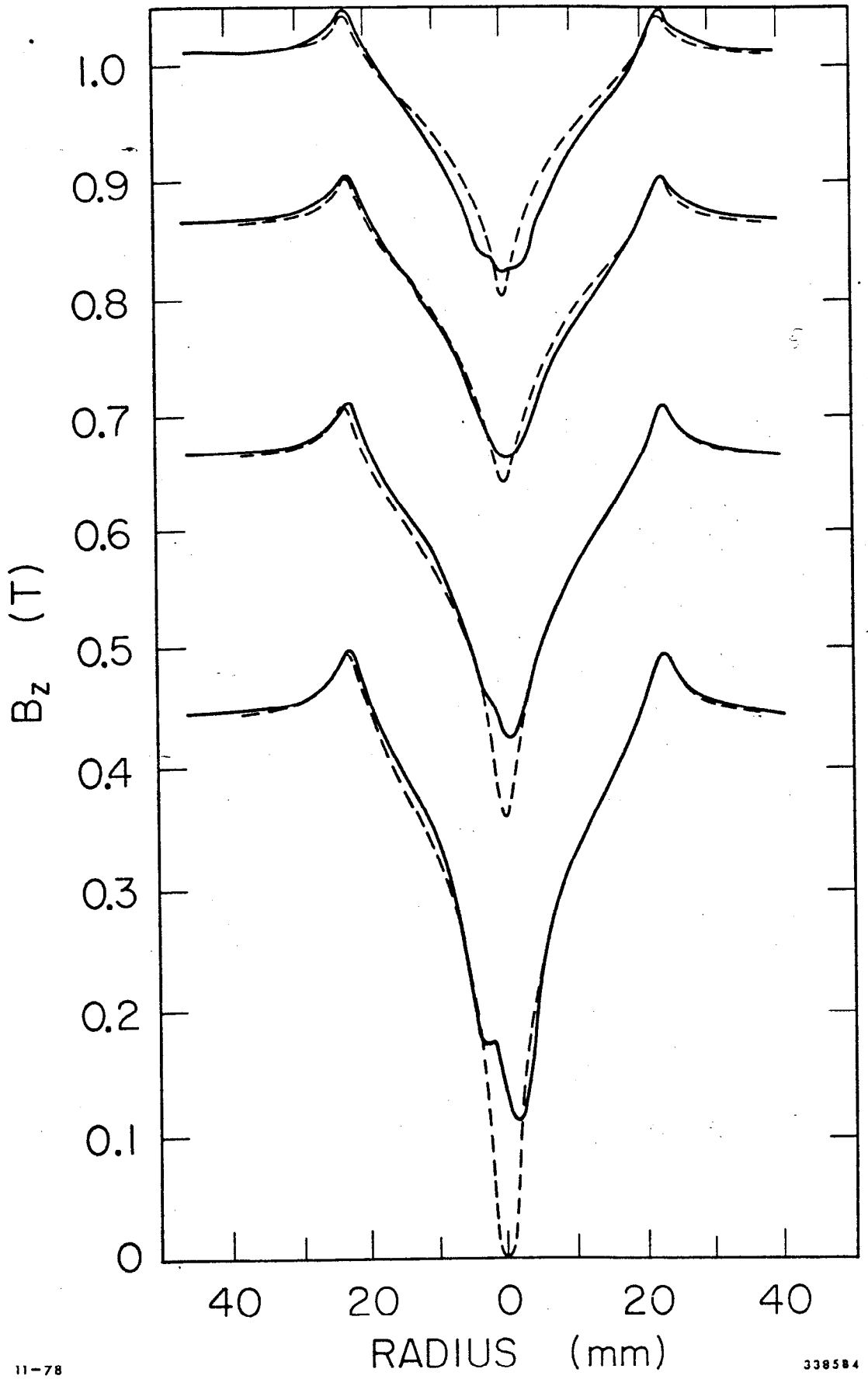
1.0
0.9
0.8
0.7
0.6
0.5
0.4
0.3
0.2
0.1
0
B_z (T)
40
20
0
20
40
RADIUS (mm)
11-78
338584

Fig. 5

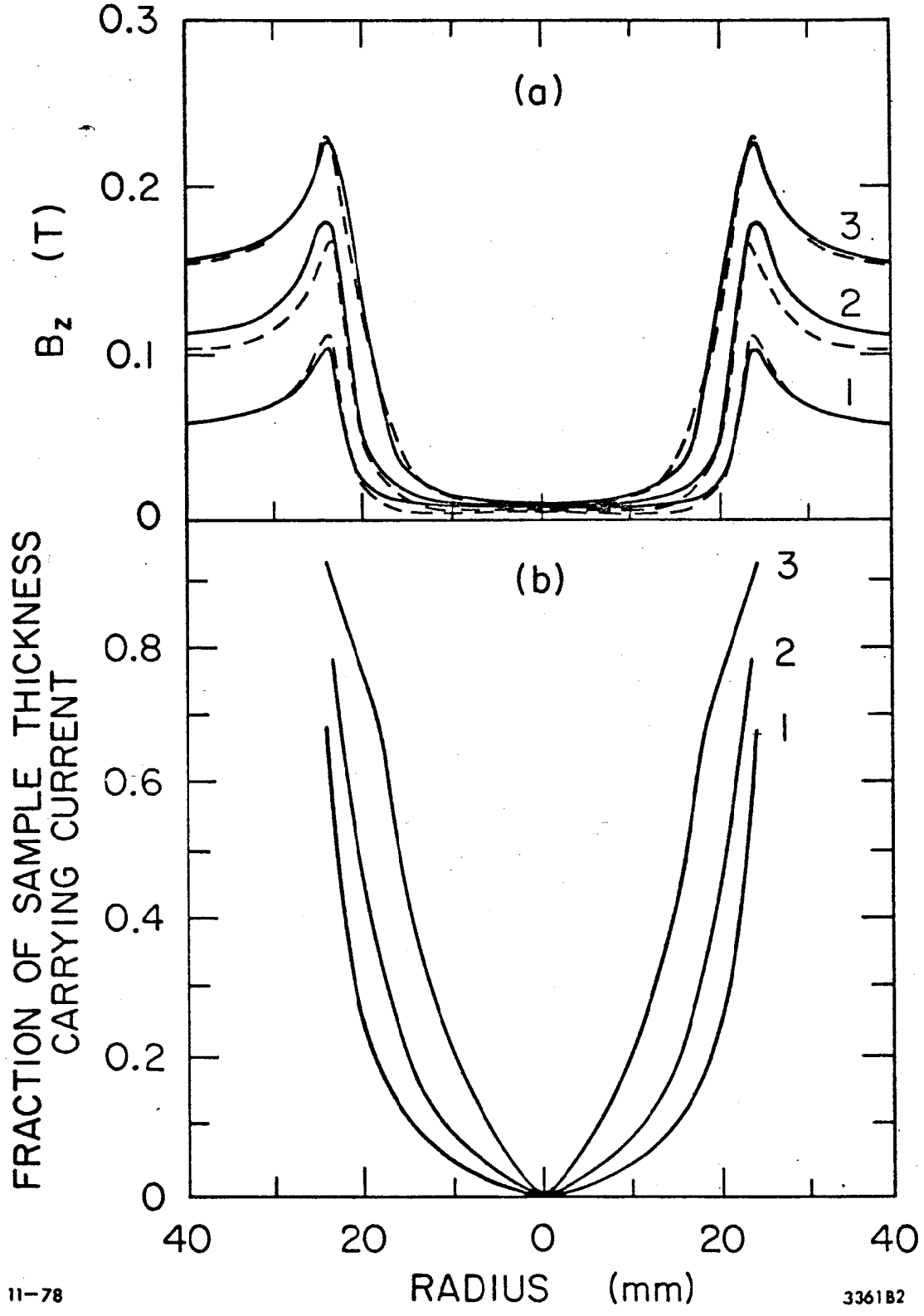
0.3
0.2
0.1
0
(a)
B_z (T)
3
2
1
(b)
0.8
0.6
0.4
0.2
0
FRACTION OF SAMPLE THICKNESS CARRYING CURRENT
40
20
0
20
40
RADIUS (mm)
11-78
3361B2

Fig. 6

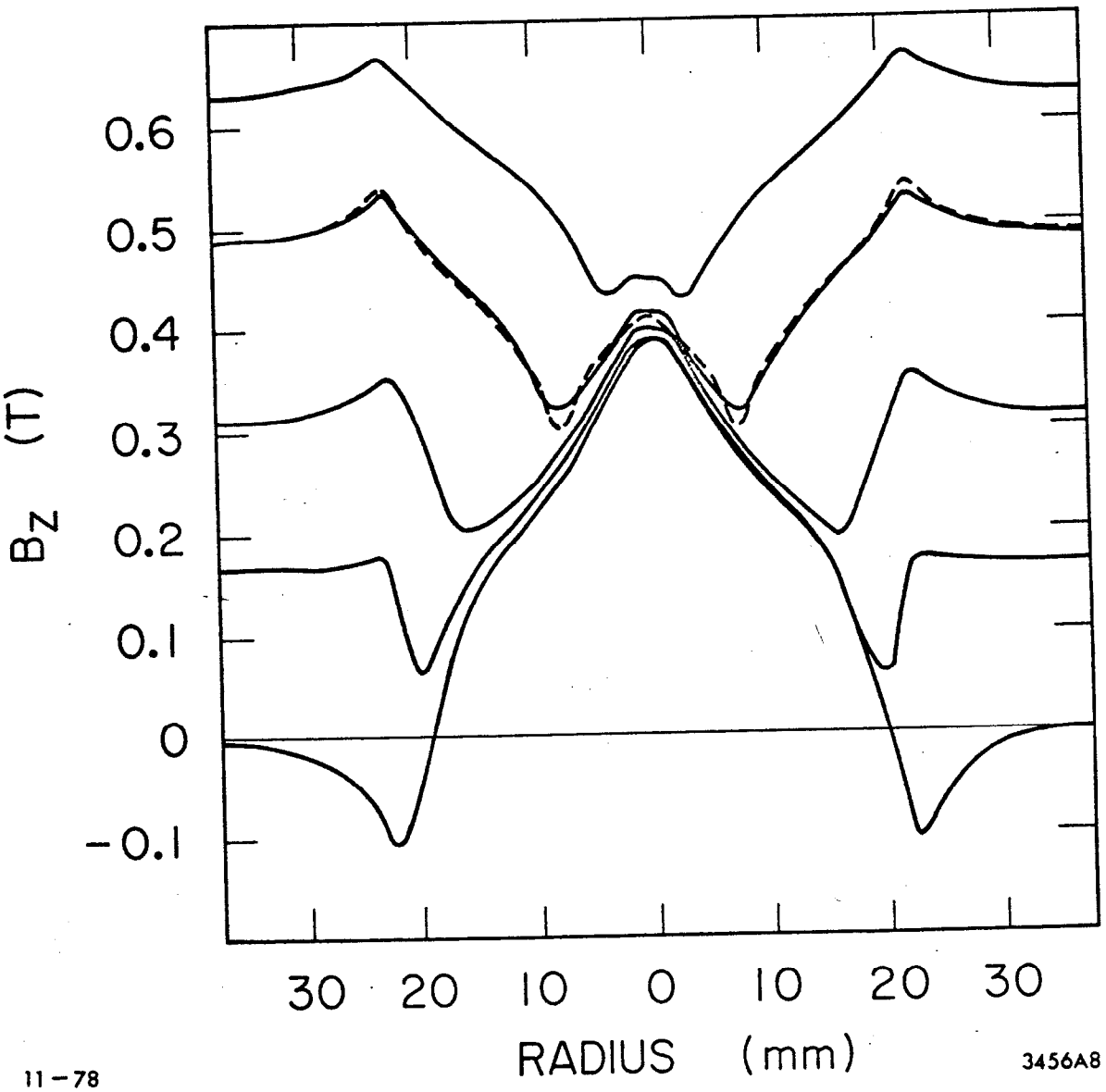

Fig. 7